MICROMACHINED STIMULATING MICROELECTRODE ARRAYS

Quarterly Report #6

(Contract NIH-NINDS-NO1-NS-9-2304)

July – September 2000

Submitted to the

Neural Prosthesis Program
National Institute of Neurological Disorders and Stroke
National Institutes of Health

by the

Center for Integrated MicroSystems
Department of Electrical Engineering and Computer Science
University of Michigan
Ann Arbor, Michigan
48109-2122

November 2000

MICROMACHINED STIMULATING MICROELECTRODE ARRAYS

Summary

This contract seeks to develop a family of thin-film stimulating arrays for use in neural prostheses. STIM-2B/-3B are two- and three-dimensional arrays of stimulating sites on 400µm centers. The probes have four channels and 64-sites. Any selected site can be used for either recording or stimulation. Current generation is off-chip. The high-end probes STIM-2/-3 are similar except they use on-chip current generation via 8-bit digital to analog converters.

During the last quarter, we continued to fabricate passive stimulating and recording probes for a wide variety of users. Yield is now high and the process is being run on a regular basis by our technical engineering staff. We have etched out a number of STIM-2B/-3B probes in preparation for a series of in-vivo experiments with these devices. Testing is a special challenge prior to microassembly in 3D arrays, and the use of special micromachined multi-contact jigs is proposed to allow contact to all sites and control leads after the release etch and before assembly. Compliant-contact jigs are being developed. A number of 256-site four-probe 3D arrays have been assembled and are ready for experiments in mapping connections between dorsal cochlear nucleus and inferior colliculus in guinea pig. Some of these experiments will be carried out during the coming quarter.

We have continued to develop the circuitry needed to operate these active stimulating probes in a wireless mode using telemetry mounted on the platform. We have now designed and fabricated the power supply generator/regulator, clock recovery circuit, data detection circuit, and the power-on-reset function using the same UM 3µm BiCMOS process used for the probes themselves. The vertical npn and pnp bipolar devices have been carefully characterized for use in these circuits as have the Zener diodes available in the process. Two voltage regulators have been developed, one producing a fixed 10V supply and another generating both 5V and 10V (or ±5V) outputs. The latter is especially attractive for the present stimulating probes, which use two supplies, and for probes employing closed-loop recording amplifiers, which also need the second supply. These circuits occupy approximately 4mm^2 in 3µm features and dissipate about 25mW. Nearly all of the power dissipation is in the voltage regulator. During the coming term, we hope to complete the design of the remaining telemetry circuits and start another fabrication run of the remaining components.

MICROMACHINED STIMULATING MICROELECTRODE ARRAYS

1. Introduction

The goal of this contract is the development of active multi-channel arrays of stimulating electrodes suitable for studies of neural information processing at the cellular level and for a variety of closed-loop neural prostheses. The probes should be able to enter neural tissue with minimal disturbance to the neural networks there and deliver highly-controlled (spatially and temporally) charge waveforms to the tissue on a chronic basis. The probes consist of several thin-film conductors supported on a micromachined silicon substrate and insulated from it and from the surrounding electrolyte by silicon dioxide and silicon nitride dielectric films. The stimulating sites are activated iridium, defined photolithographically using a lift-off process. Passive probes having a variety of site sizes and shank configurations have been fabricated successfully in past contracts and have been distributed to a number of research organizations nationally for evaluation in many different research preparations. For chronic use, the biggest problem associated with these passive stimulating probes concerns their leads, which must interface the probe to the outside world. Even using silicon-substrate ribbon cables, the number of allowable interconnects is necessarily limited, and yet a great many stimulating sites are ultimately desirable in order to achieve high spatial localization of the stimulus currents.

The integration of signal processing electronics on the rear of the probe substrate (creating an "active" probe) allows the use of serial digital input data which can be de-multiplexed on the probe to provide access to a large number of stimulating sites from a very few leads. Our goal in this area is to develop a family of active probes capable of chronic implantation in tissue. For such probes, the digital input data must be translated on the probe into per-channel current amplitudes that are then applied to tissue through the sites. Such probes generally require five external leads, virtually independent of the number of sites used. As discussed in previous reports, we have designed a series of active probes containing CMOS signal processing electronics. Two of these probes have been completed and are designated as STIM-1A and STIM-1B. A third probe, STIM-2, is now beginning a final iteration and is a second-generation version of our original high-end first-generation design, STIM-1. All three probes provide 8-bit resolution in digitally setting the per-channel current amplitudes. STIM-1A and -1B offer a biphasic range using ±5V supplies from 0µA to ±254µA with a resolution of 2µA, while STIM-2 has a range from 0 to ±127µA with a resolution of 1µA. STIM-2 offers the ability to select 8 of 64 electrode sites and to drive these sites independently and in parallel, while STIM-1A allows only 2 of 16 sites to be active at a time (bipolar operation). STIM-IB is a monopolar probe, which allows the user to guide an externally-provided current to any one of 16 sites as selected by the digital input address. The high-end STIM-2 contains provisions for numerous safety checks and for features such as remote impedance testing in addition to its normal operating modes. It also offers the option of being able to record from any one of the selected sites in addition to stimulation. It will be the backbone of a

multi-probe three-dimensional (3D) 1024-site array (STIM-3) now in development. A new probe, STIM-2B, has recently been added to this set. It offers 64-site capability with off-chip generation of the stimulus currents for four separate channels. These channels are organized in four groups so that each current can be directed to any of the 16 sites in its group. Each selected channel can be programmed for either stimulation or recording. On-chip recording amplifiers offer a gain of 50; alternatively, the neural activity can be recorded using off-chip amplifiers interfaced through the normal stimulating channels. This probe is available in both 2D and 3D versions (as STIM-2B/3B) and is now being used in-vivo.

During the past quarter, we have continued to fabricate passive probe structures for a wide variety of users. Additional STIM-3B probes have been fabricated and assembled into fully-functional 256-site four-probe arrays. Testing these probes prior to assembly is an important challenge, and several new approaches to speeding up this process have been considered. Circuits for a telemetry interface for the active probes have been designed and fabricated using the 3µm UM BiCMOS process and have been extensively tested. The results in each of these areas are described more fully in the sections below.

2. Passive Probe Developments

Passive probes, primarily for recording but with some targeted at stimulating applications or for use in conjunction with multi-point sttimulation, continue to be distributed to investigators in the U.S. and abroad under the NCRR-funded Center for Neural Communication Technology. In addition to distributing standard designs from the CNCT catalog, the CNCT offers a custom design service to advanced probe users and collaborators. New mask sets are typically fabricated on a yearly basis. The most recent mask set, CNCT5, has just been fabricated to completion. It includes designs for Wayne Aldridge, Sandy Bledsoe, John Middlebrooks and Erich Staudacher of the University of Michigan, David Edell of InnerSea Technology, Chris Hempel of Brandeis University, Daryl Kipke of Arizona State University, Mark Knuepfer of St. Louis University, Charles Miller and Paul Abbas of the University of Iowa and Christophe Pouzat of Caltech. Some of these designs will be described and shown below.

Dr. Aldridge's probe, the tip of which is shown in Fig. 1, is designed for chronic recording from substantia nigra pars reticulata in the freely-behaving rat. With this new design, Dr. Aldridge will examine the differences in recording longevity between sites along the edge, sites that protrude over the edge and sites at the tip of the substrate. As described in an earlier report in the companion recording contract, we are investigating the possibility of extending recording lifetime by taking advantage of relative movement at the brain/probe interface and its potential to provide a "cleaning" effect of the probe surface. Dr. Aldridge has already successfully recorded activity for the 29 days required by his experiment using side sites on another probe design.

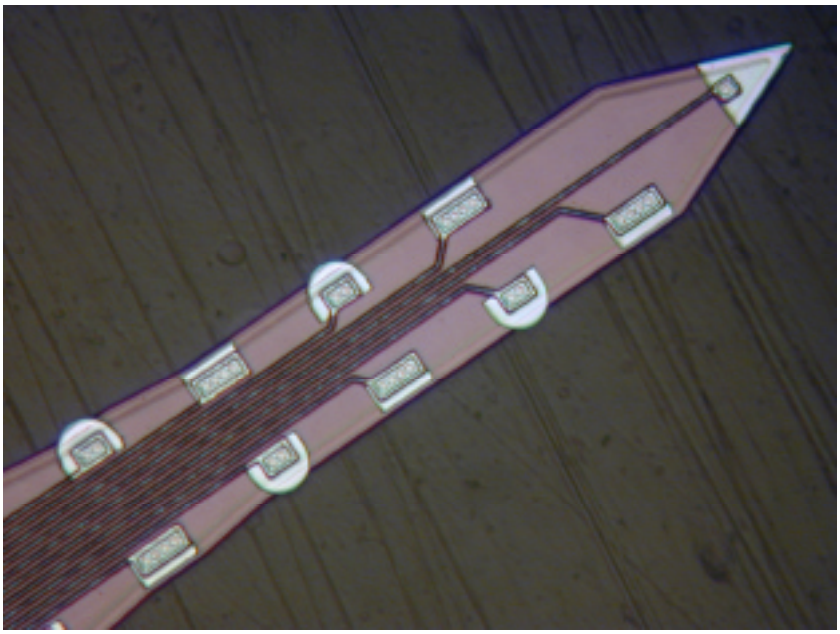

Fig. 1: Tip of a probe fabricated for Wayne Aldridge of the University of Michigan for chronic recording from rat substantia nigra pars reticulata. The effects of site placement on recording longevity will be evaluated. Sites along the edge are spaced on 80µm centers.

Two probes fabricated for Dr. Kipke's work are shown in Fig. 2. The 8-shank design is for chronic recording from rat auditory cortex and the 2-shank design is for chronic recording in monkey motor cortex. Each probe has 32 sites with varying surface areas. The ribbon cables on these probes are angled to permit clearance of the skull with a normal placement of the probe in tissue. A new connector assembly is being designed to accommodate the angled cable and the increased channel density.

Two new acute probe designs from CNCT5 are shown in Fig. 3. The left probe, fabricated for Dr. Hempel from the laboratory of Sacha Nelson, was designed for recording from rat visual cortex slices. The right probe was designed by Dr. Bledsoe for acoustic mapping in the guinea pig inferior colliculus. Both probes have 32 sites. The CNCT is receiving an increasing number of requests for probes with higher channel counts. New acute packages are being developed to decrease the size of the standard 16-channel connector as well to increase the channel count.

A photograph of the probe fabricated for Drs. Miller and Abbas for acute mapping of cat auditory nerve is shown in Fig. 4. This probe has a combination of design features (such as site area and tip shape) that were taken from a variety of other probes that were used in preliminary tests. The sites and shanks are spaced to permit a spatial survey of excitation from a large cross section of the nerve.

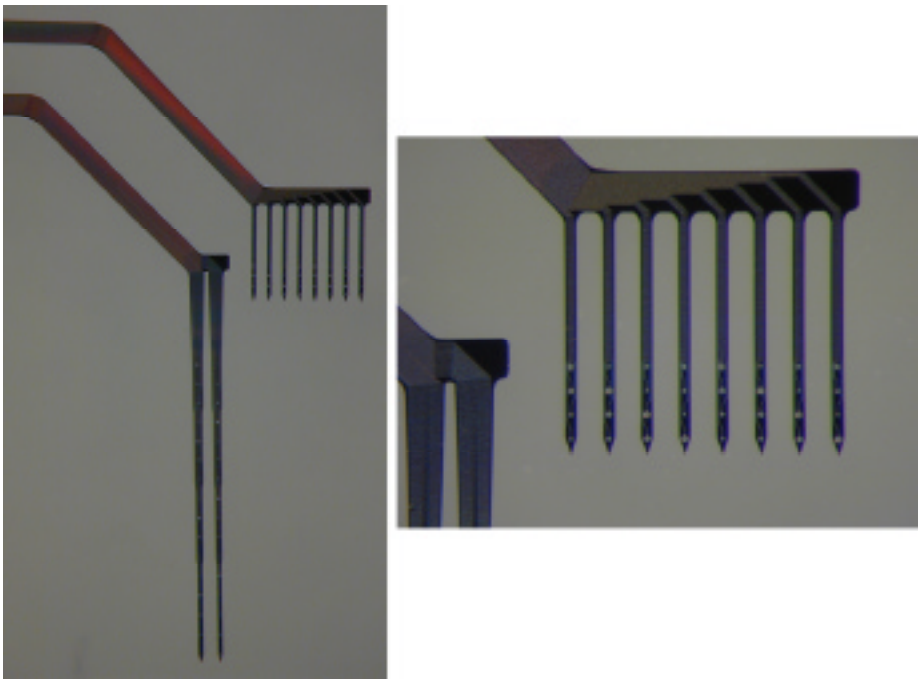

Fig. 2: Probes fabricated for Dr. Kipke for use in monkey motor cortex (2-shanks) and rat auditory cortex (8-shanks). The angled cables will permit clearance of the skull once the probes are inserted. The shanks on the monkey probe are spaced at 250µm and on the rat probe at 200µm.

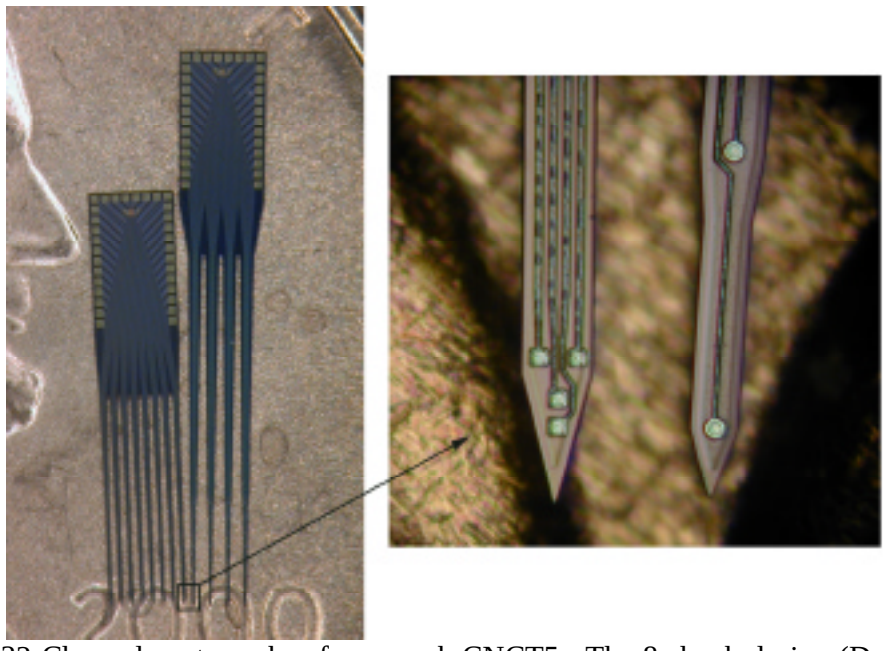

Fig. 3: 32-Channel acute probes from mask CNCT5. The 8-shank design (Dr. Hempel) has a tetrode at each shank tip as shown in the inset. Shanks are spaced at 150µm. Each shank on the 4-shank design (Dr. Bledsoe) has 8 sites spaced on 200µm centers, while the shanks themselves are spaced at 250µm.

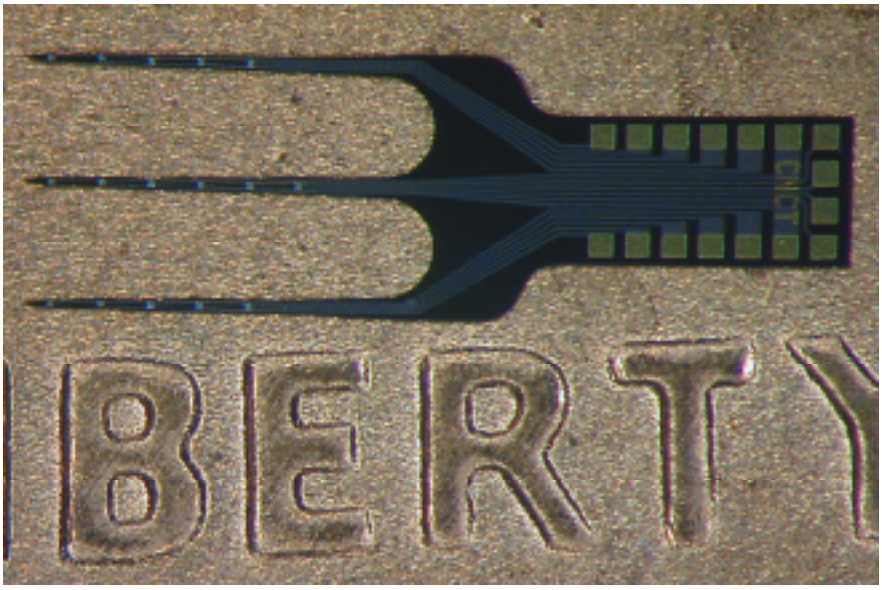

Fig. 4: Probe fabricated for Drs. Miller and Abbas for recording from cat auditory nerve. The spacing between shanks (500µm) and sites (200µm) were chosen to permit a spatial sampling from a large portion of the nerve.

2. Active Stimulating Probe Development

Recent active stimulating probe development has focused on the assembly and use of 3D stimulating arrays (Stim-3B). We have assembled several of the 3D arrays of different sizes. We have worked out some of the difficulties in the assembly process. We have also performed more *in-vivo* experimental work in which we exercised the entire External User Interface system, including the GUI and the headstage electronics.

STIM-2B/3B

The STIM-2B/3B probes are expected to prove to be very useful tools in the study of the central nervous system because of the large area of tissue that these probes can instrument. The devices are quite simple, and their function and design has been discussed extensively in previous quarterly reports. STIM-2B is an acute 2D structure that functions by simply clocking in 20 bits of data. These bits are used to decode the four site addresses. The addressed sites are connected via an analog multiplexer to an input/output (I/O) pad which is driven from an external current source. A single flag bit is bundled with the site address and when set enables a simple amplifier which can be used for recording activity at the site in lieu of stimulation. STIM-3B is an extension of STIM-2B, altered just enough to make it compatible with a 3D array. This includes some structural modifications such as outriggers with gold beam-lead interconnects and slotted wings which mate with micromachined spacers. There is only a small addition in the circuitry: a 4b register and a second 4-channel analog multiplexer. The 4b register is loaded with data that controls whether the individual channels of the probe are gated onto

the platform I/O bus (via a probe address). The other significant feature of STIM-3B is that the 4b register is serially connected to the 4b registers of the other probes in the 3D array. This allows all of the probes to be addressed simultaneously with a single lead. This architecture helps reduce the number of leads required for the array.

During the past quarter, work has progressed on development of the 3D probe arrays. Many of the STIM-3B probes had previously been etched out with the STIM-2B probes. The STIM-3B probes were comprehensively tested by manually probing each of the iridium stimulating sites on a probe station. As mentioned in the previous report, this process is very time consuming and can take several hours per device tested. The STIM-3B probes have the added complexity of additional circuitry and additional leads to be tested. These most recent tests were performed utilizing the new headstage which includes the capability to easily measure and monitor the current supplied by the power supplies. Typical 'good' probes have static power supply currents less than 1μA. Several of the tested probes, while fully functional, had static power supply currents greater than 100μA. The exact cause of the large supply current is not known although it is likely due to a processing defect in the circuitry. While not significant so long as the device functions properly; in the future, this type of problem must be screened in testing since a large power draw can not be tolerated in wireless implants. The capabilities of the monitoring circuitry may prove very beneficial in this testing aspect as well. We are looking into various ways to automate the testing process since it is very important to be completely sure that each probe is fully functional before assembling it into a 3D array. The problem is that truly comprehensive manual testing is very time consuming.

We have also worked on assembling arrays of different sizes (different numbers of probes) with varying amounts of success. We have identified several difficulties that arise during the assembly process and developed improvements to that process. With each additional array assembled, we are learning better and more reliable techniques of assembly. Figure 5 shows one fully-assembled array. Figure 6 shows an enlargement of the beam-lead interconnect area on one end of the platform. The beam-leads were laid out in pairs, as can be seen in Fig. 7, since we were not certain of the reliability and yield of the 90^{o} beam-lead interconnect technique. Our experience to date has indicated that this redundancy is not necessary and should not be included in future designs. Including only one beam lead per interconnection will help in reducing the overall size of the array.

Failure of a single beam (one half of the pair) lead has yet to occur. There has only been one instance of a beam-lead failure in the probes tested, in which case the entire beam pair popped loose from the wing. There was apparently some processing defect because a problem with this interconnect showed up during previous testing as high resistance, which would indicate a problem in the contact and/or adhesion of the beam. This was a very isolated case since the adjacent leads did not fail and functioned normally, and the problem has not been observed on any other probe.

We have also used the platform fuses to program the platforms for different numbers of probes. The fuses normally short the X-DATA IN pad of a 2D array to the X-DATA OUT pad so that when an array is not present, the data can still propagate to the

next array position on the platform. By applying a voltage across the fuse, the gold heats up and melts, 'blowing' the fuse and leaving an open-circuit that then forces the X-DATA address to propagate through the array at that position before proceeding to the next array position. Figure 8 shows one of these platform fuses after it has been 'blown'.

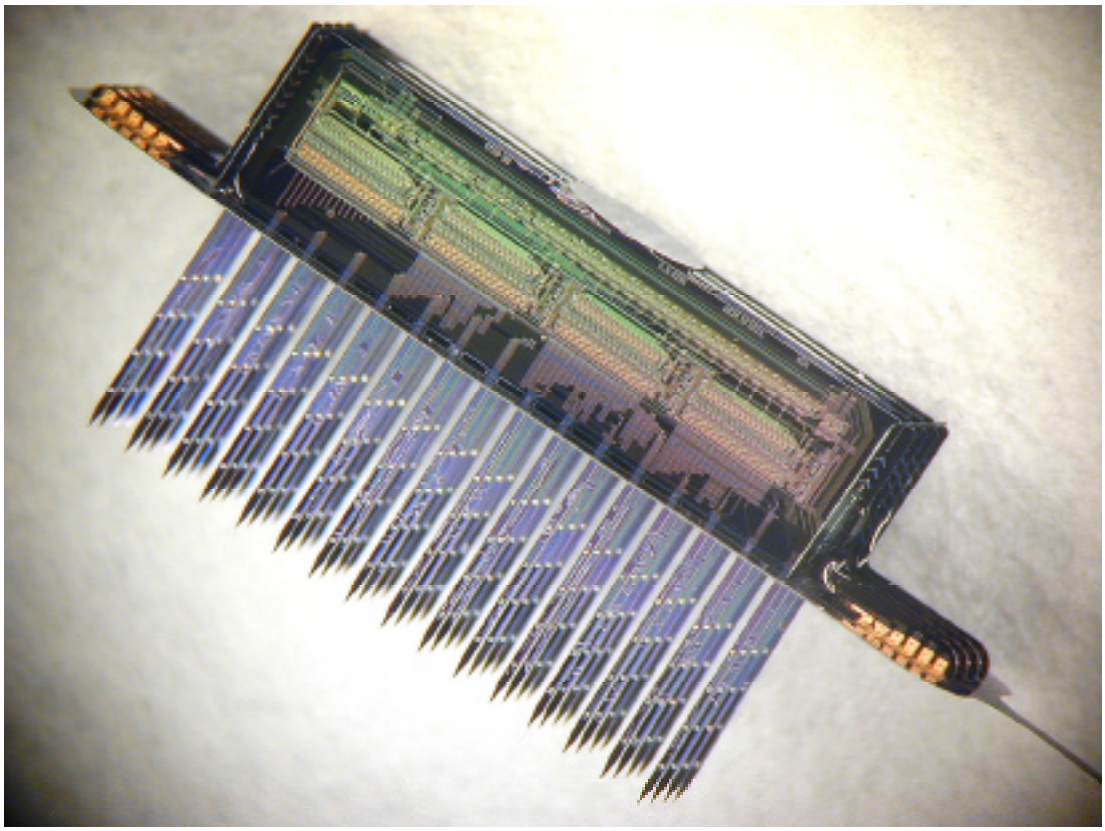

Fig. 5: A completed 4-channel, 256-site, 3D STIM-3B stimulating probe.

We have also worked on evaluating the stimulating probes by looking at the mapping of the auditory tract from the dorsal cochlear nucleus to the inferior colliculus. This has been the first time we've attempted to use the complete external user interface system including the new headstage with its voltage to current converter, output buffers, probe power supply monitors, etc. Use of the new system has introduced problems of its own, but it appears to function for the most part as expected. Some problems have been found in the system which are being worked out, but none of them have kept us from using the system. Thus far the results of these experiments have been unsuccessful mainly because of the difficulty in getting the rather large arrays properly positioned into the dorsal cochlear nucleus of a guinea pig. There are also some issues that are being worked out so that existing hardware for recording can be readily connected to the recording outputs of STIM-3B for simultaneous and synchronized recording.

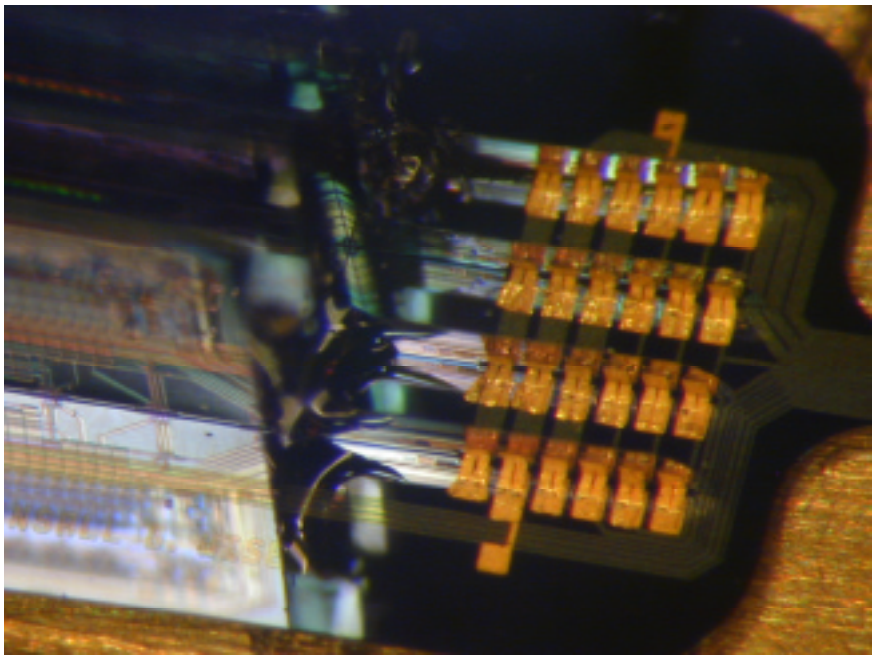

Fig. 6: A microscope photograph of the 4 rows of 90° gold beam-lead interconnects from the individual 2D probe arrays to the common platform in STIM-3B.

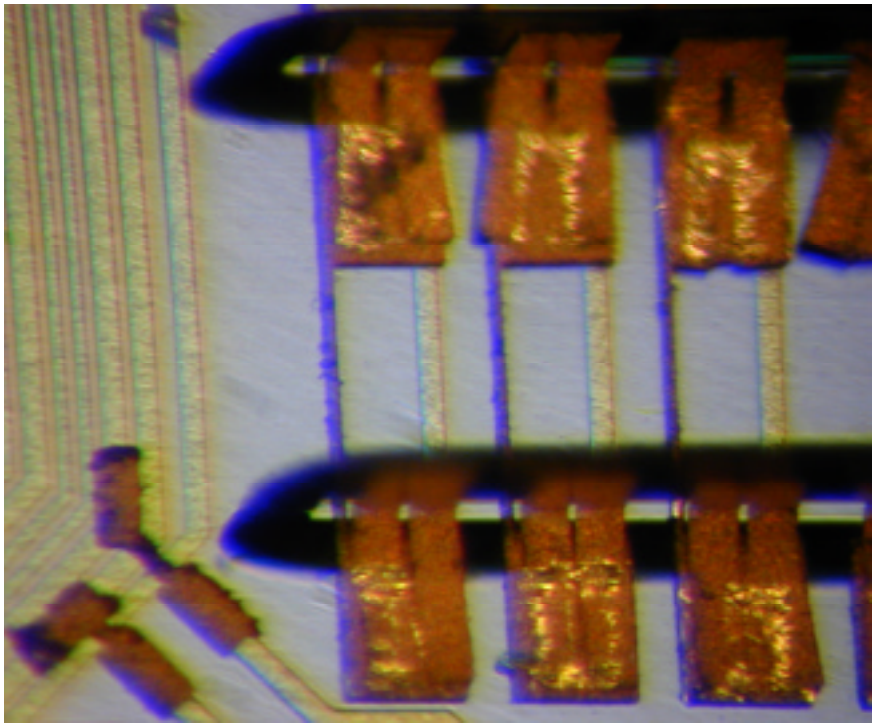

Fig. 7: A close-up view of several of the paired 5μm-thick gold beam leads which show the marks of being already bonded. The beam leads interconnect the outriggers of the 2D probes and mating bondpads on the platform.

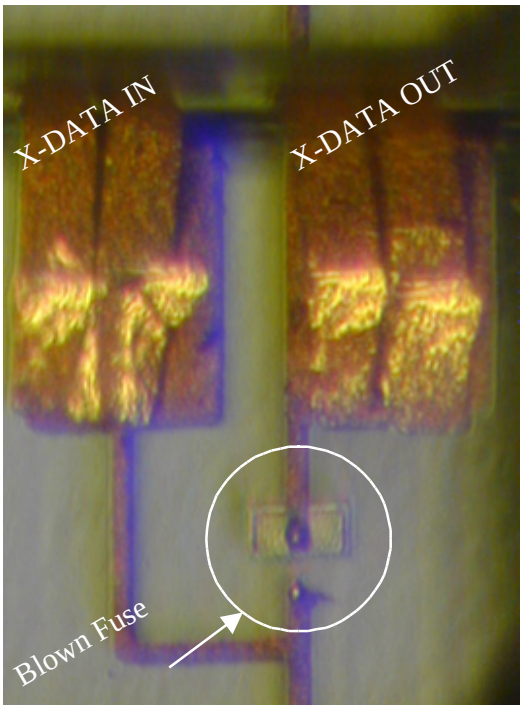

Fig. 8: A close-up view of one of the integrated fuses on the platform. Because a probe has been placed at this position, the fuse has been blown in order to disconnect the X-DATA IN pad from the X-DATA OUT forcing the 3D address data through the probe.

The system appears to be functioning correctly; the stimulus artifact moves as expected as the stimulus is cycled through the various sites of the array. Unfortunately, thus far, a driven response at the recording electrodes has not yet been achieved, probably due to improper probe positioning. The relatively large size of the arrays compared to the small target in a guinea pig brain makes it a somewhat difficult approach. We anticipate that by making improvements in our approach and with continuing experience, we will be able utilize this type of experiment very successfully to demonstrate the flexibility and usefulness of these arrays.

One other difficulty that we have observed is that while the headstage is relatively compact, it still provides a rather large obstruction when trying to visualize the *in-vivo* preparation under a microscope. We believe that with proper layout and use of a commercial PCB manufacturer, we should be able to shrink the size of the headstage down to half its current size. In the future, we plan to do this, but we want to continue to use the current headstage until we feel all the problems are known and we understand all of the changes that need to be made.

In preparation for these experiments, the probes to be used were activated and CV's were measured across the array in accordance with our continuing observation of the ability to activate iridium sites in parallel. In spite of the likelihood of there being

some difference in site access resistances due to variations in on-chip lead resistance, the sites appear to activate to within a few percent of each other in terms of their charge capacity.

In order to increase our supply of the STIM-3B probes, we have also etched out more these probes. The number of probes required for assembling 3D arrays makes it very important to continue adding to our supply of working probes on hand. We have also etched out more of the 3D array structural pieces so that we can continue to assemble the 3D STIM-3B probe arrays. During the coming quarter, we anticipate assembling more 3D probe arrays and plan to continue our *in-vivo* experimental efforts. We are also looking at performing some simple *in-vitro* experiments to look at the feasibility of using active stimulating and recording electrodes in the same experiment. The ability to use the two types of probes in the same *in-vitro* preparation may also have some implications in automated testing methods.

One Possible Test Strategy

As indicated above, testing the active probes is time consuming and some means of comprehensive testing after the release etch and before assembly into a 3D array is badly needed. The process should allow access to all of the sites at the same time as well as to the power and output leads. One possible approach is described here.

In 3D arrays, the beam lead transfers are bent in a micromachined jig similar to that shown in Fig. 9. The mold in the jig is 15um deep defined by the probe shape mask and is used for holding the probe in place while a piece of glass is used to clamp the upper part of probe firmly in position. If an electrode array corresponding to the site array can be formed in the mold for the probe shanks, simultaneous access to all the sites should be possible, as shown in Fig.10.

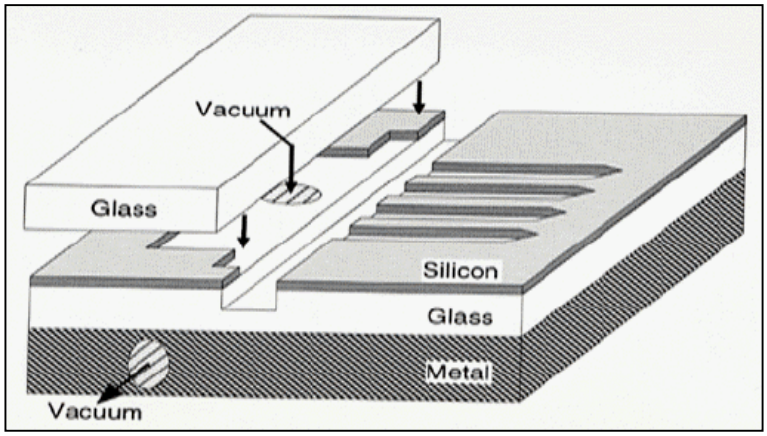

Fig 9: Perspective view of a micromachined jig for bending beam lead transfers in a 3D array.

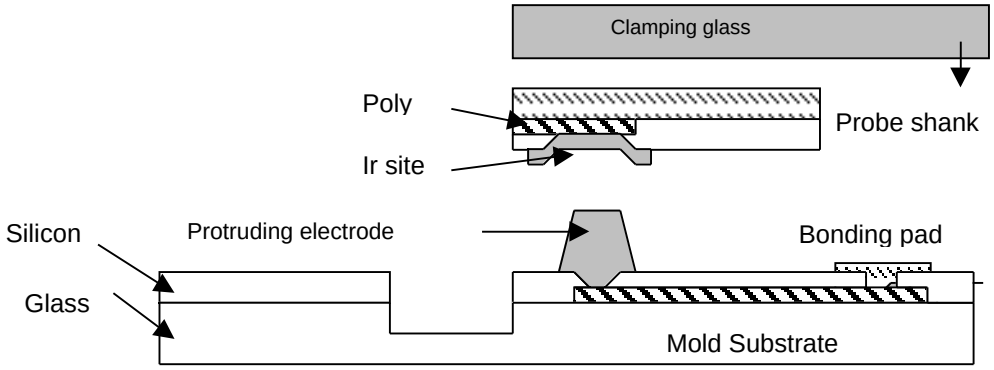

Fig. 10: Cross-sectional view of a protruding electrode on a micromachined testing jig and corresponding site on the probe shank.

Only one protruding electrode and its corresponding site are shown in the figure for simplicity. Thus, for each probe, a test jig would be designed along with it to allow testing. Extra masks would certainly be needed, but it would do much to speed up the overall process. A drawback in this scheme is the difficulty in making contact to all points simultaneously, i.e., the height of all substrate bumps will not be identical and unless they have some degree of compliance they will never all make contact at the same time. In order to allow the necessary motion, it should be possible to fabricate the contacts using a surface-undercut structure, allowing vertical motion on the contact bumps. This can either be done using cantilevers as shown in Fig. 11 or as double-end-clamped beams (to allow greater stiffness and contacting force). Such structures will be explored further during the coming term.

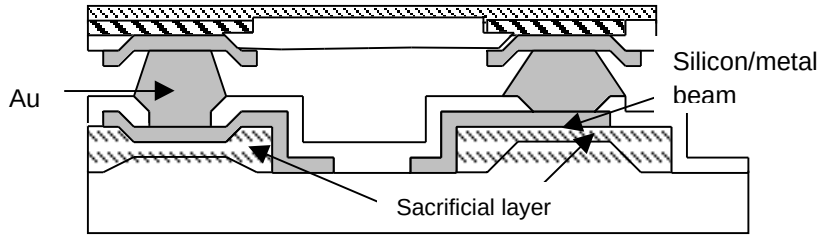

Fig. 11: A method for pressure-contacting the finished probe prior to bonding using a test jig with cantilevered compliant contacts.

4. A Telemetry-Powered CNS Stimulating System

During the past quarter, fabrication of the circuit blocks needed in the wireless interface circuit chip was completed using the 3μm UM-BiCMOS process. This chip operates multi-channel stimulating probes using a telemetry link. Figure 12 shows the

Wireless CNS Stimulating System and the role of the interface circuit chip. The fabricated circuit blocks include: 1) the power supply generator/regulator, 2) clock recovery circuit, 3) data detection circuit, and 4) the power-on-reset function. A block diagram of the interface chip is shown in Fig. 13, with the implemented blocks shown in darker color. Design of these circuit blocks is based on similar blocks designed for implantable muscular stimulators, but with several modifications to improve performance or reduce power dissipation.

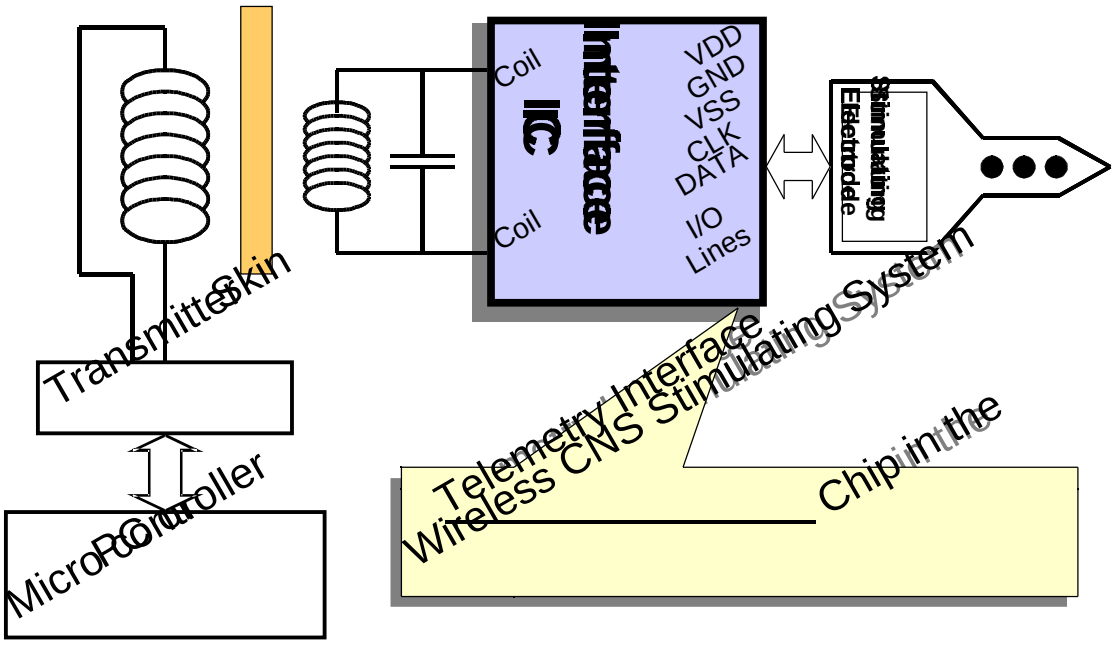

Fig. 12: Telemetry interface chip in the wireless stimulating system.

One of the differences between the circuitry used for these CNS probes and the circuitry used for functional neuromuscular stimulators (FNS) is the circuit fabrication technology. The silicon probes utilize a BiCMOS process that incorporates deep boron diffusion, which is needed to form the probe substrate, whereas FNS systems use a standard BiCMOS process without deep boron diffusion. Since only one process is run for the silicon probes, the telemetry circuit layouts were included in the same set of masks and protection against the final EDP release etch step was included. This also required us to modify and compile a new set of device and circuit parameters for use in the circuit simulator SPICE. Using these new parameters, the different circuit blocks were designed and simulated. To experimentally derive these new parameters, a test bench was included in the layouts, which contains a full set of the devices used in our circuits with different sizes and geometries. What follows is a summary of the wafer-level tests conducted on some of the more critical test devices and the four fabricated circuit blocks mentioned above.

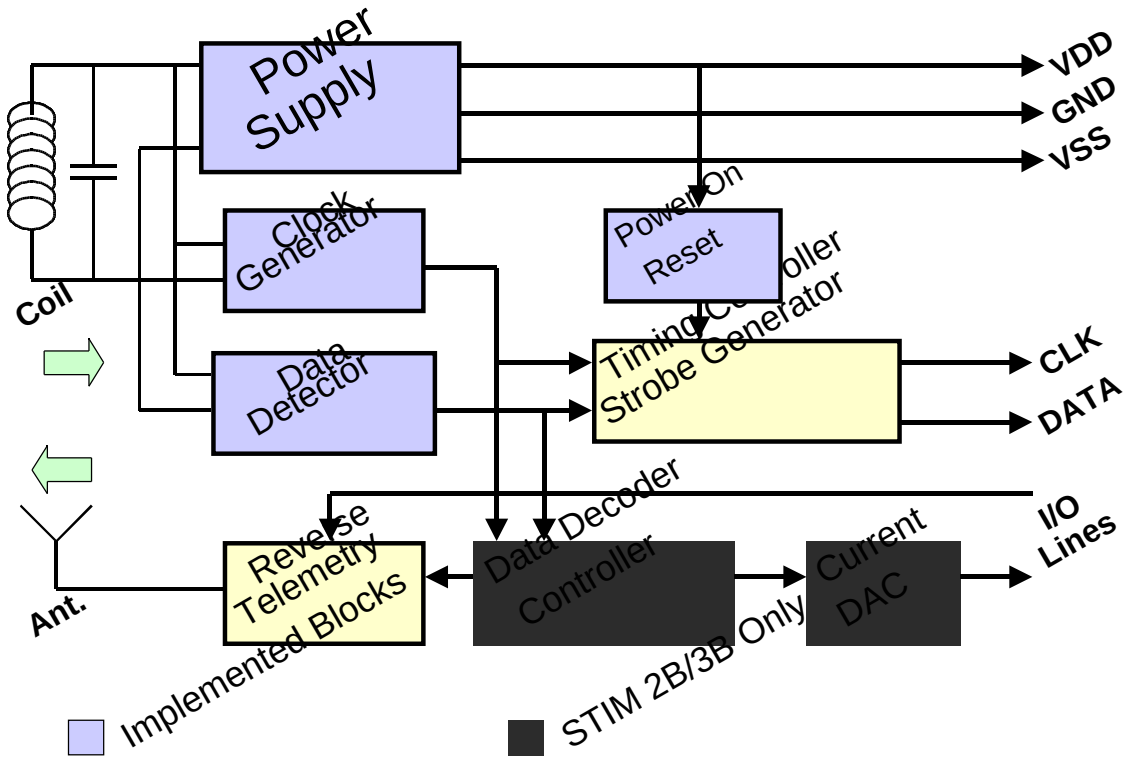

Fig. 13: The telemetry interface chip block diagram

Vertical NPN Bipolar Junction Transistor and Diode:

Figure 14 shows the cross-section of a vertical NPN transistor, including its parasitic components. The main use of these transistors is as BJT diodes in the full-bridge rectifier of the regulator block. Since our process lacks an N+ buried layer between the N-substrate and the N-epi, R_{epi}, the collector parasitic resistor value, can be quite significant. When a large current passes through the diode, There will be a voltage drop across the collector resistor determined by the N-epi doping and transistor geometry that is shown in Fig. 15. This voltage drop will induce a voltage across the base-emitter junction of the vertical PNP BJT and can cause this transistor to turn on and steal current from the diode to the grounded substrate. This is why all the BJT diodes and transistors should be properly sized due to their maximum collector currents; otherwise, a great deal of power will be wasted through parasitic devices. The vertical PNP transistor standard I-V characteristics and its forward current gain variation with collector current are shown in Fig. 16. Figure 17 shows the I-V characteristics of two BJT diodes with different geometries. These diodes can be modeled by an ideal diode in series with a resistor. diode parameters are shown in Table 1.

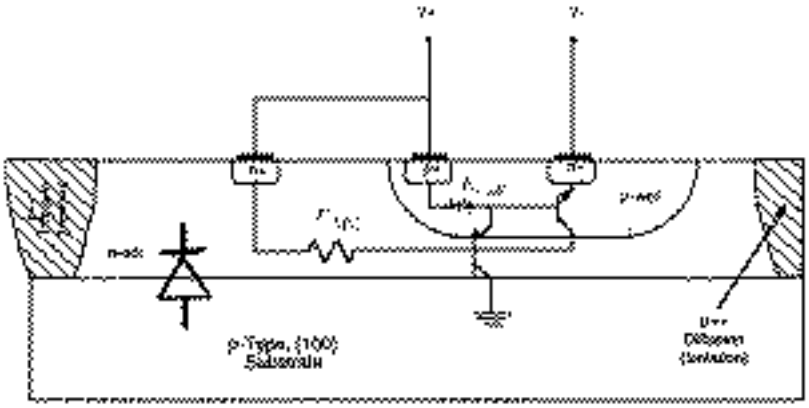

Fig. 14: Cross sectional view of a vertical NPN transistor including its parasitic effects.

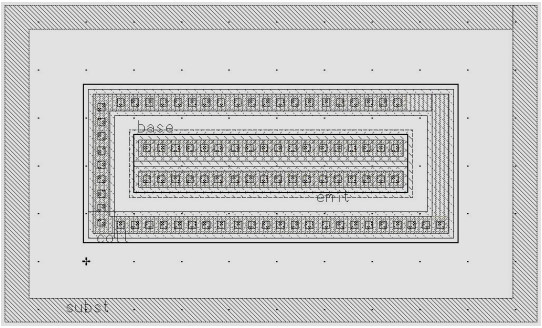

Fig. 15: Layout of a vertical NPN transistor including its isolating deep boron ring.

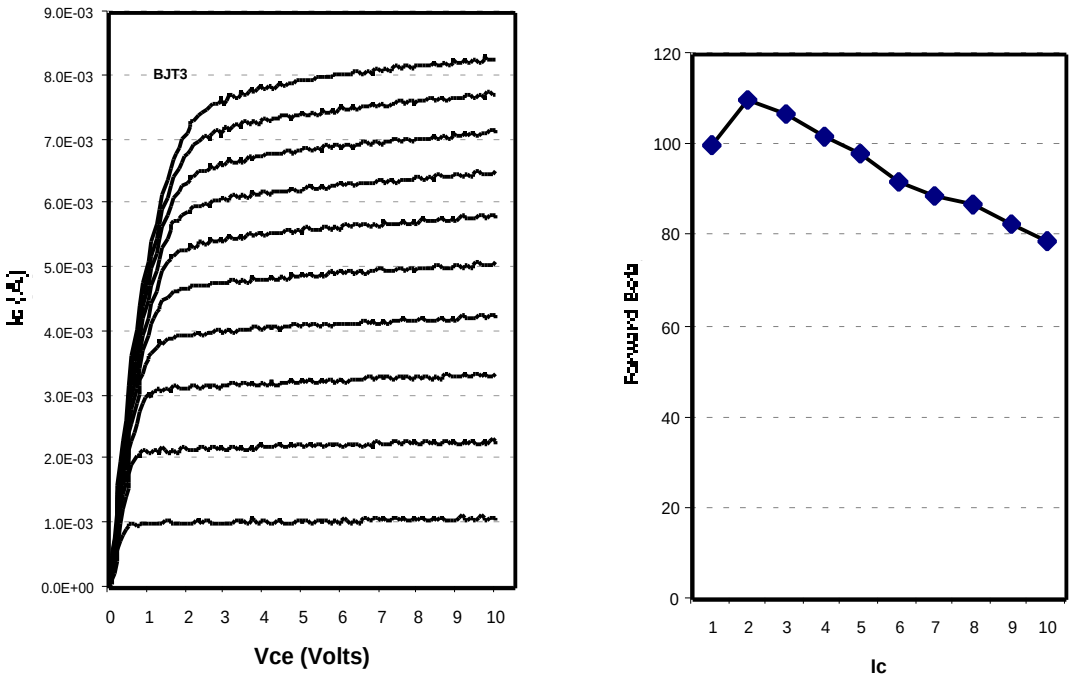

Fig. 16: Vertical NPN transistor I-V characteristics and beta variations with collector current.

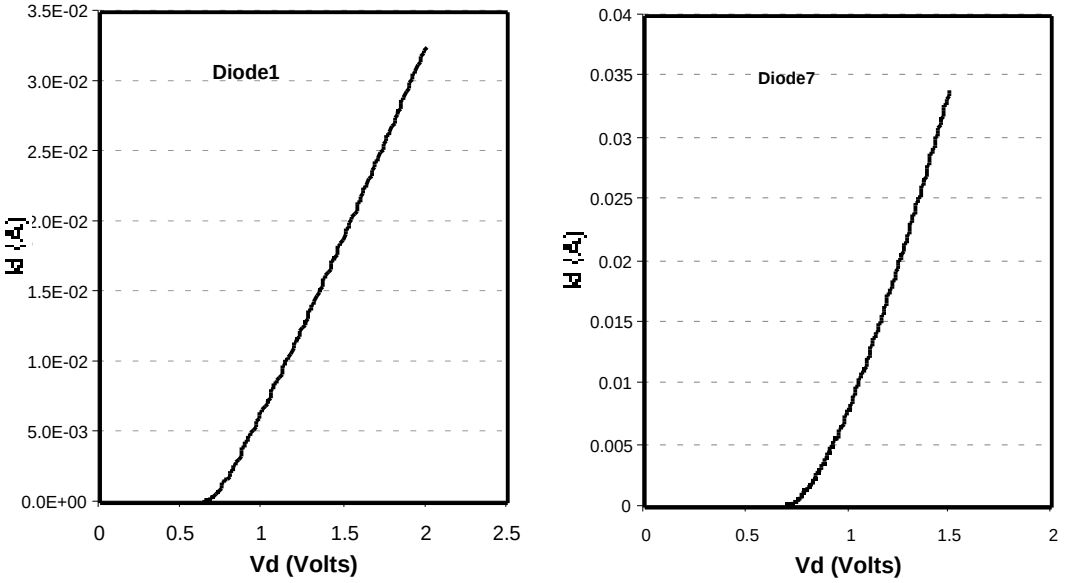

Fig. 17: BJT diode I-V characteristics with different geometries.

Table 1: BJT diode parameters

Name	**Collector Size**	**Series Resistance (Ohm)**	**Reverse Breakdown Voltage (V)**	**Saturation Reverse Current (A)**
Diode1	75x58 µm	37.3	20.5	1.65e-15
Diode7	300x58 µm	19.91	23.1	1.60e-16

Zener Diodes:

Zener diodes are used in the power supply circuit to regulate the output voltage around 5V and 10V. Three different Zener diodes with different geometries were designed and tested. Figures 18 and 19 and Table 2 show their I-V characteristics, layouts, and circuit parameters, respectively. By comparing Zener characteristics in Table 2, it can be concluded that Zener 5 is the best choice for regulator applications; Zener 1B is suitable when a low current reference is needed.

Table 2: Zener diode parameters.

Name	**Zener Breakdown (V)**	**Forward Series Resistance (Ohm)**	**Reverse Series Resistance (Ohm)**
Zener1A	5.0~5.3	29.9	241
Zener1B	5.3	27.9	226
Zener5	5.43	17.5	29.5

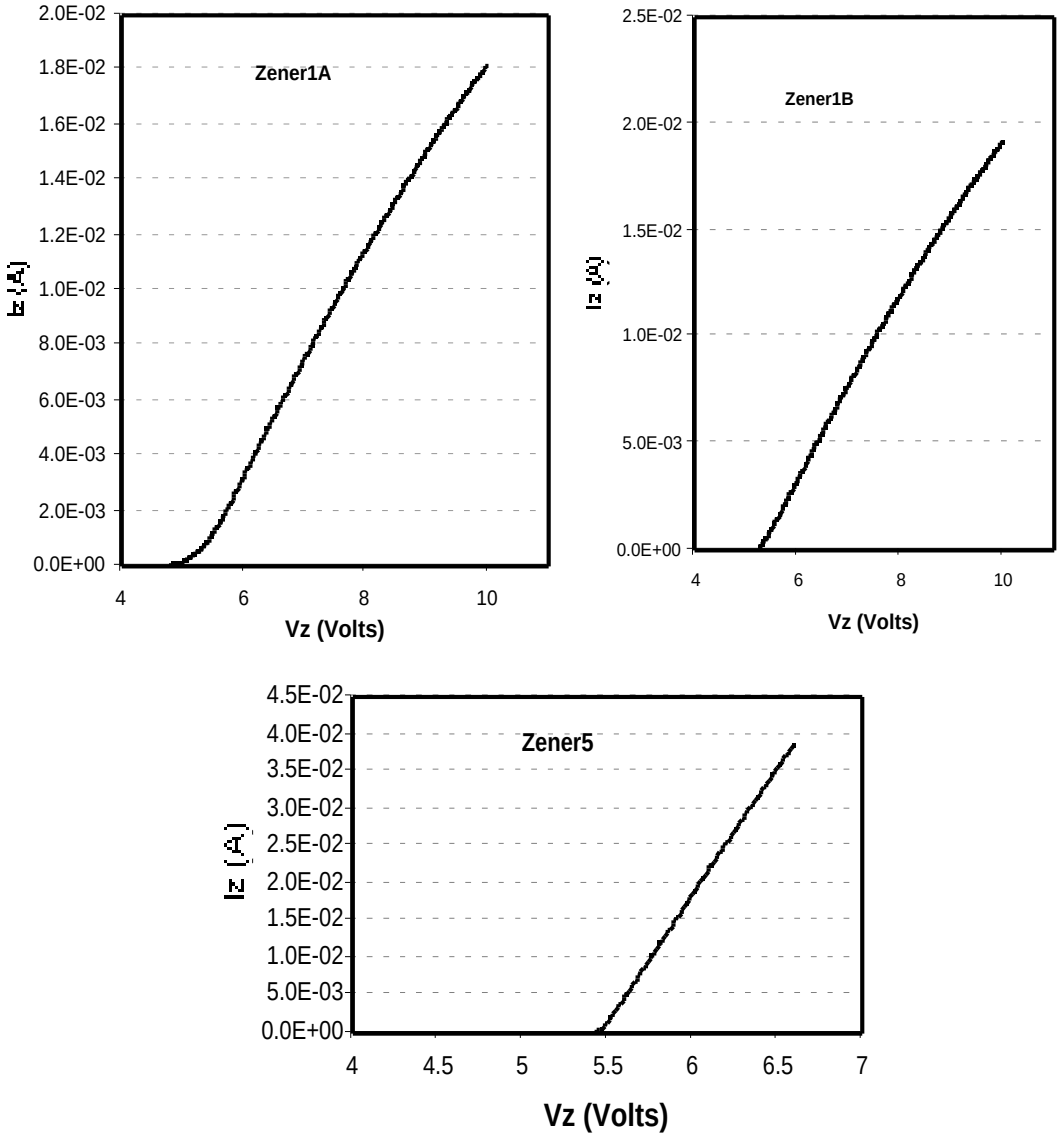

Fig. 18: Zener diode I-V characteristics.

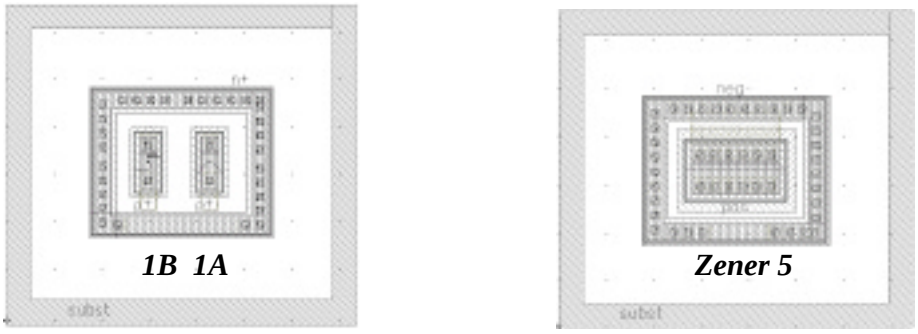

Fig. 19: Zener diode layouts with different geometries.

Voltage Regulators:

A die photograph of two voltage regulators is shown in Fig. 20. The voltage regulator on the left only has a single 5V output, but the regulator on the right produces two output voltages, 10V and 5V, and its design is an improved version of the regulator circuit designed for the FINESS chip. The 10V supply is used for stimulating current sources which need to overcome high stimulating site impedance and should have a large compliance voltage to inject enough current into tissue. The 5V supply is used for the rest of the circuit blocks. A modification of the 5V supply is shown in Fig. 21. By adding a push pull class AB output stage to the original 5V supply, the new design can source and sink as much 5mA. This output can be used as the circuit ground for the stimulator chip, thus producing both positive and negative 5V supplies in order to support previous active multi-channel stimulating probes, such as STIM2 and 2B, that require dual supplies.

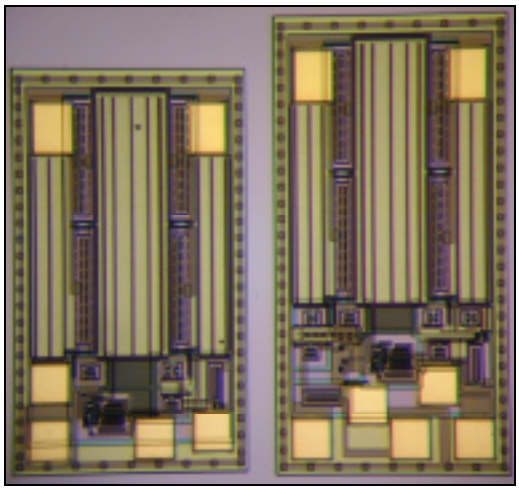

Fig. 20: Die photomicrograph of the 5V single output and 10V dual output voltage regulators.

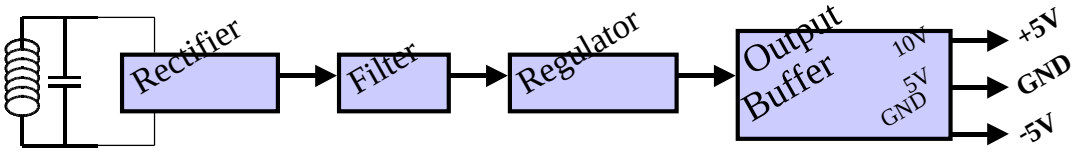

Fig. 21: Dual output regulator block diagram used as a dual supply.

The voltage regulators were tested using a hard-wired signal generator. In these first experiments a wireless link was not utilized. Under the actual operational condition the receiver coil is isolated from the circuit ground by the rectifier bridge diodes. Under test conditions, the signal generator was not isolated from the circuit ground, and so the

signal generator signal cannot go below ground. In order to correct for this, a DC voltage was added to the 10V peak-peak input carrier to eliminate negative input voltage. This means only one of the diodes in the bridge was used as a half wave rectifier.

Figure 22 compares experimental and simulated regulator performance, showing regulator output voltage as a function of DC input voltage. One of the reasons for the fairly large difference between simulated and actual load regulation is the Zener diode used in the circuit. The Zener diode used in this circuit was of type 1A, which according to Fig. 18 has the worst I-V characteristics and the highest parasitic series resistance compared to type 1B or Zener 5. We expect to obtain better voltage regulation by replacing these Zener diodes in the modified designs. Another deviation from regulator simulation results was the much higher measured power dissipation and input current. This is believed to be due to substrate leakage current in the bridge rectifier BJT diodes. Figure 23 shows a square relationship between the regulator power consumption and its input voltage when supplying a 5.4KΩ load.

The 5V output of the dual supply regulator was measured to be lower than the expected value. Its no-load voltage was 4.13V which dropped to 3.5V when loaded with a 5.4KΩ resistor. This is mainly because the 5V output has been taken from the 10V output through a 20KΩ resistor. The actual value of this resistor is much larger than the required value due to the processing parameter variations. In new designs this resistor has been omitted and the 5V output is directly taken from a Zener reference.

Power-On-Rest:

Figure 24 shows the die photomicrograph of the power-on reset (POR) block needed to reset the entire system when it is powered up. This monostable circuit guarantees the digital circuitry and registers always start from a known reset state. This signal not only resets the interface chip internal circuitry but also resets all the connected stimulating probes. A measured waveform for this circuit is shown in Fig. 25. A 10pF capacitor is linearly charged through a current source after applying power, decreasing the input voltage of a Schmitt trigger stage and finally changes its output state.

Figure 26 shows the power-on delay and power-on reset current consumption as a function of supply voltage. These curves can be used to adjust the size of the delay capacitor in order to achieve a desired amount of power-on delay.

Clock Recovery:

The clock recovery die photomicrograph is shown in Fig. 27. In this circuit a capacitive voltage divider synchronizes a ring oscillator with the half-rectified carrier signal. This circuit should be functional over a wide input range of received carrier amplitudes from 8V to 35V peak. Table 3 summarizes the measurements made on this block with 3 different supply voltages. It can be seen that the circuit current consumption increases rapidly as the supply voltage increases. Figure 28 shows the measured waveform for the clock output (top trace), and sinusoidal input signal (bottom trace).

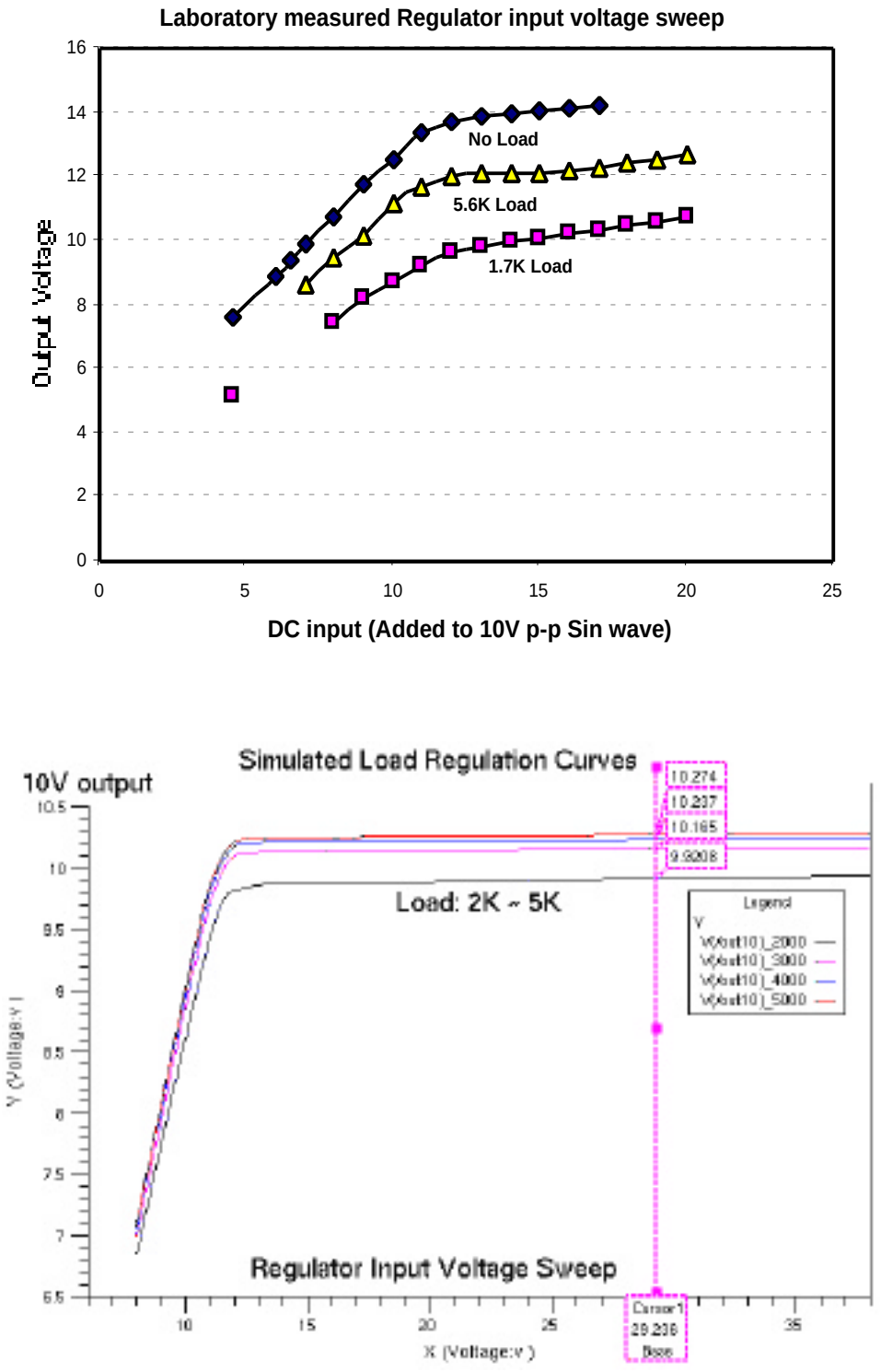

Fig. 22: Measured and simulated regulator output voltage versus applied input voltage.

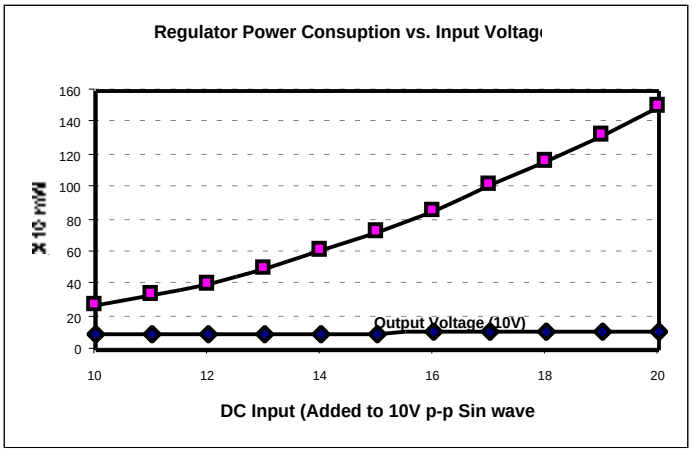

Fig. 23: Regulator power consumption vs. input voltage supplying a 5.4KΩ load.

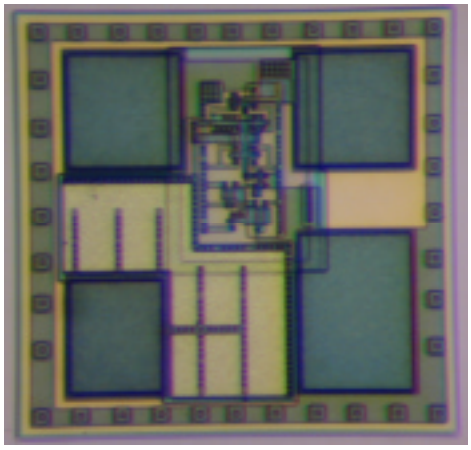

Fig. 24: Die photomicrograph of the power-on-reset block

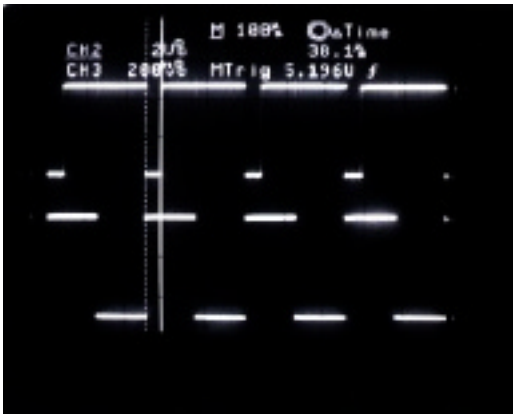

Reset Pulse Output

Power on Input

Fig. 25: Power-on-reset measured waveforms.

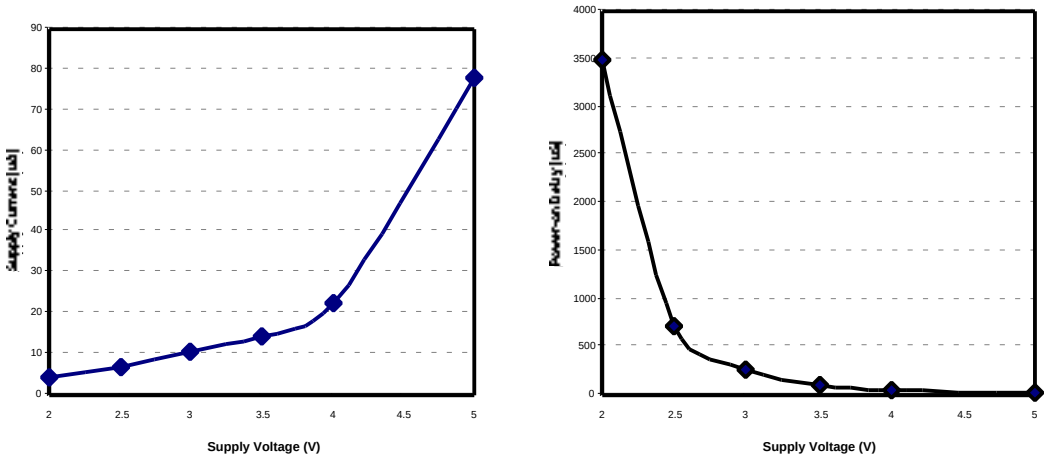

Fig. 26: Power-on delay and current consumption as a function of supply voltage.

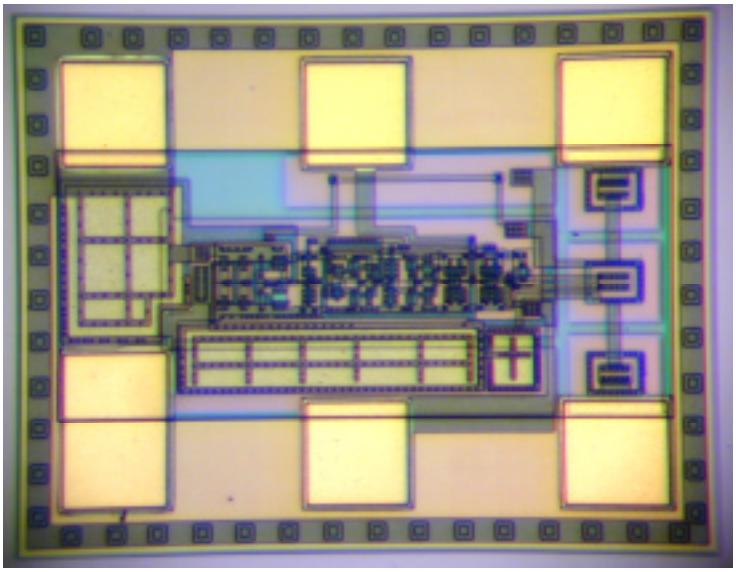

Fig. 27: Die photomicrograph of the clock recovery block.

Table 3: Clock recovery block performance with changing supply voltage

Supply Voltage (V)	Ring Oscillator Frequency (MHz)	Minimum Carrier Freq.	Maximum Carrier Freq.	Supply Current (mA)
2.5	1.0	1	5	0.77
3.5	1.43	1	10	1.57
5	1.76	1	12.5	3

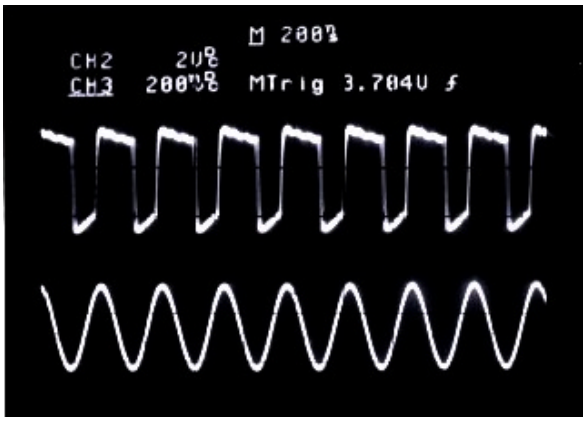

Fig. 28: Measured input and output waveforms for the clock recovery circuitry.

Data Detector:

The data detector die photomicrograph is shown in Fig. 29. The amplitude-modulated rectified carrier is passed through a bandpass filter to remove the DC offset and the high-frequency carrier. Then a Schmitt trigger converts the analog signal to a PWM semi-digital bit stream. The switching levels of the Schmitt trigger stage should be chosen carefully based on the carrier modulation, but they also vary considerably with supply voltage. This problem caused the chip to work only in a small range of supply voltages around 2V. Modulation depth can be as low as 30% but lowering the modulation depth limits circuit functionality and supply range. Another drawback of this design is its limited baud rate, which is only 16Kbit per second and is not enough for large number of sites in multi-site stimulating probes. This circuit will be replaced by a faster circuit with enough provisions for the Schmitt trigger switching level adjustment.

The measured waveforms for the data detector are shown in Fig. 30. In this test each frame consists of 16 bits and the frame rate is 1K frame per second. The beginning of each frame is specified by a square pulse.

Table 4 shows a summary of the size and average power consumption of the fabricated circuit blocks. The minimum and maximum power consumption is measured with 2.5V and 5V supply voltages, respectively. Die areas include the pads added to each individual block for input and output access. Most of these pads will be omitted in the final interface chip layout, in which all the blocks are internally wired so we expect to achieve a 30% reduction in total die area.

During the coming quarter, other circuit blocks of the wireless stimulating system shown in Fig. 13 will be designed and simulated. These test results will be used to optimize and modify the above circuits as well as new designs. Additional tests will be conducted on the regulator blocks using isolated coils and measuring substrate currents to precisely locate the most power consuming elements in these circuits. And finally new layouts will be designed for the next fabrication run.

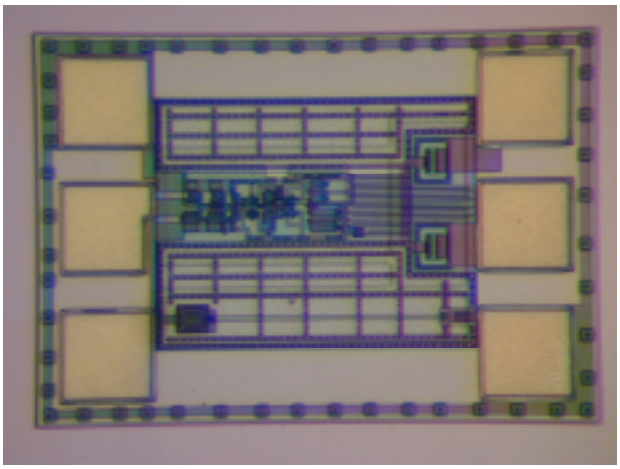

Fig. 29: Die photomicrograph of the Data Detector block.

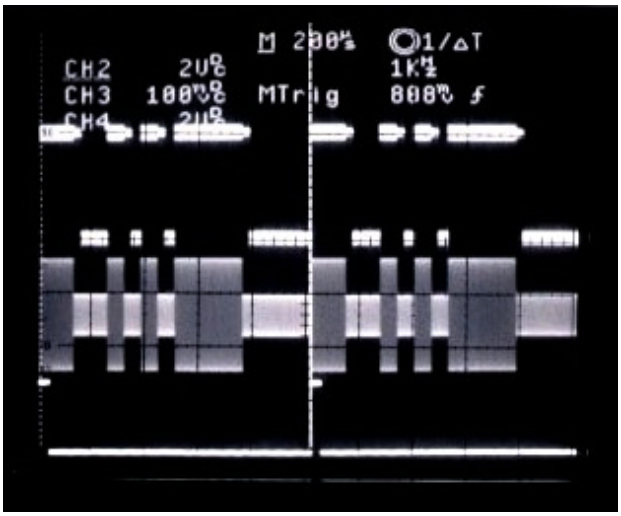

Fig. 30: Measured waveforms for the data detector circuitry.

Table 4: Performance summary of fabricated circuit blocks.

Circuit Block	**Die Area mm^2**	**Max(Min) Power mW**
10/5V Regulator	1.36	45 (23)
5V Regulator	1.10	32 (18.5)
Clock Generator	0.71	7 (0.35)
Data Detector	0.66	5.5 (0.31)
Power On Reset	0.25	0.39 (0.05)

6. Conclusions

During the last quarter, we continued to fabricate passive stimulating and recording probes for a wide variety of users. Yield is now high and the process is being run on a regular basis by our technical engineering staff. We have etched out a number of STIM-2B/-3B probes in preparation for a series of in-vivo experiments with these devices. Testing is a special challenge prior to microassembly in 3D arrays, and the use of special micromachined multi-contact jigs is proposed to allow contact to all sites and control leads after the release etch and before assembly. Such compliant-contact jigs are being developed. A number of 256-site four-probe 3D arrays have been assembled and are ready for experiments in mapping connections between dorsal cochlear nucleus and inferior colliculus in guinea pig. Some of these experiments will be carried out during the coming quarter.

We have continued to develop the circuitry needed to operate these active stimulating probes in a wireless mode using telemetry mounted on the platform. We have now designed and fabricated the power supply generator/regulator, clock recovery circuit, data detection circuit, and the power-on-reset function using the UM 3µm BiCMOS process used for the probes themselves. The vertical npn and pnp bipolar devices have been carefully characterized for use in these circuits as have the Zener diodes available in the process. Two voltage regulators have been developed, one producing a fixed 10V supply and another generating both 5V and 10V (or ±5V) outputs. The latter is especially attractive for the present stimulating probes, which use two supplies, and for probes employing closed-loop recording amplifiers, which also need the second supply. These circuits occupy approximately 4mm2 in 3µm features and dissipate about 25mW. Nearly all of the power dissipation is in the voltage regulator. During the coming term, we hope to complete the design of the remaining telemetry blocks and start another fabrication run of the remaining components.